Available on CMS information server

CMS NOTE 2006/143

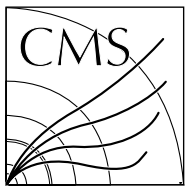

The Compact Muon Solenoid Experiment

CMS Note

Mailing address: CMS CERN, CH-1211 GENEVA 23, Switzerland

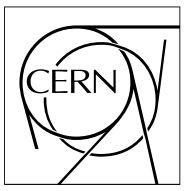

27 May 2007

Energy Response and Longitudinal Shower Profiles Measured in CMS HCAL and Comparison with GEANT4

CMS HCAL Collaboration

G. Baiatian, A. Sirunyan

Yerevan Physics Institute, Yerevan, Armenia

I. Emeliantchik, V. Massolov, N. Shumeiko, R. Stefanovich

NCPHEP, Minsk, Belarus

J. Damgov, L. Dimitrov, V. Genchev, S. Piperov, I. Vankov

Institute for Nuclear Research and Nuclear Energy, Bulgarian Academy of Science, Sofia, Bulgaria

L. Litov

Sofia University, Sofia, Bulgaria

G. Bencze, A. Laszlo, A. Pal, G. Vesztergombi, P. Zalan

KFKI-RMKI, Research Institute for Particle and Nuclear Physics, Budapest, Hungary

A. Fenyvesi

ATOMKI, Debrecen, Hungary

H. Bawa, S. Beri, V. Bhatnagar, M. Kaur, J. Kohli, A. Kumar, J. Singh

Panjab University, Chandigarh, 160 014, India

B. Acharya, Sud. Banerjee, Sun. Banerjee, S. Chendvankar, S. Dugad, S. Kalmani, S. Katta, K. Mazumdar, N. Mondal, P. Nagaraj, M. Patil, L. Reddy, B. Satyanarayana, S. Sharma, K. Sudhakar, P. Verma

Tata Institute of Fundamental Research, Mumbai, India

M. Hashemi, M. Mohammadi-Najafabadi, S. Paktinat

Institute for Studies in Theoretical Physics and Mathematics and Sharif University of Technology, Tehran, Iran

I. Golutvin, V. Kalagin, I. Kosarev, V. Ladygin, G. Mescheryakov, P. Moissenz, A. Petrosyan, S. Sergeyev, V. Smirnov, A. Vishnevskiy, A. Volodko, A. Zarubin

JINR, Dubna, Russia

V. Gavrilov, Y. Gershtein[1)], N. Ilyina, V. Kaftanov, I. Kisselevich, V. Kolossov, A. Krokhotin, S. Kuleshov, D. Litvintsev[2)], A. Ulyanov, G. Safronov, S. Semenov, V. Stolin

ITEP, Moscow, Russia

A. Demianov, A. Gribushin, O. Kodolova, S. Petrushanko, L. Sarycheva, V. Teplov, I. Vardanyan, A. Yershov

Moscow State University, Moscow, Russia

V. Abramov, P. Goncharov, A. Kalinin, A. Khmelnikov, A. Korablev, Y. Korneev, A. Krinitsyn, V. Kryshkin, V. Lukanin, V. Pikalov, A. Ryazanov, V. Talov, L. Turchanovich, A. Volkov

IHEP, Protvino, Russia

T. Camporesi, T. de Visser, E. Vlassov[3)]

CERN, Geneva, Switzerland

S. Aydin, M. Bakirci, S. Cerci, I. Dumanoglu, E. Eskut, A. Kayis-Topaksu, S. Koylu, P. Kurt, G. Onengut, H. Ozkurt, A. Polatoz, K. Sogut, H. Topakli, M. Vergili, T. Yetkin

Cukurova University, Adana, Turkey

K. Cankoçak[4)], A. Esendemir, H. Gamsizkan, M. Guler, C. Ozkan, S. Sekmen, M. Serin-Zeyrek, R. Sever, E. Yazgan, M. Zeyrek

Middle East Technical University, Ankara, Turkey

M. Deliomeroglu, K. Dindar, E. Gülmez, E. Isiksal[5)], M. Kaya[6)], S. Ozkorucuklu[7)]

Bogazici University, Istanbul, Turkey

L. Levchuk, P. Sorokin

KIPT, Kharkov, Ukraine

V. Senchishin

Single Crystal Institute, Kharkov, Ukraine

J. Hauptman

Iowa State University, Ames, IA, USA

S. Abdullin, J. Elias, D. Elvira, J. Freeman, D. Green, S. Los, V. O'Dell, A. Ronzhin, I. Suzuki, R. Vidal, J. Whitmore

Fermi National Accelerator Laboratory, Batavia, IL, USA

M. Arcidy, E. Hazen, A. Heering, C. Lawlor, D. Lazic, E. Machado, J. Rohlf, F. Varela, S. X. Wu

Boston University, Boston, MA, USA

D. Baden, R. Bard, S. Eno, T. Grassi, C. Jarvis, R. Kellogg, S. Kunori, J. Mans[8)], A. Skuja

---

[1)] Now at Florida State University, Tallahassee, FL, USA.

[2)] Now at FNAL, Batavia, IL, USA.

[3)] Also with ITEP, Moscow, Russia.

[4)] At Mugla University, Mugla, Turkey.

[5)] At Marmara University, Istanbul, Turkey.

[6)] At Kafkas University, Kars, Turkey.

[7)] At Süleyman Demirel University, Isparta, Turkey.

[8)] Now at University of Minnesota, Minneapolis, MN, USA.

University of Maryland, College Park, MD, USA

V. Podrasky, C. Sanzeni, D. Winn

Fairfield University, Fairfield, CT, USA

U. Akgun, S. Ayan, F. Duru, J. Merlo, A. Mestvirishvili, M. Miller, E. Norbeck, J. Olson, Y. Onel, I. Schmidt

University of Iowa, Iowa City, IA, USA

N. Akchurin, K. Carrell, K. Gümüş, H. Kim, M. Spezziga, R. Thomas

Texas Tech University, Lubbock, TX, USA

M. Baarmand, H. Mermerkaya, R. Ralich, I. Vodopiyanov

Florida Institute of Technology, Melbourne, FL, USA

L. Kramer, S. L. Linn, P. Markowitz

Florida International University, Miami, FL, USA

P. Cushman, Y. Ma, B. Sherwood

University of Minnesota, Minneapolis, MN, USA

L. Cremaldi, J. Reidy, D. A. Sanders

University of Mississippi, Oxford, MS, USA

D. Karmgard, R. Ruchti

University of Notre Dame, Notre Dame, IN, USA

W. Fisher, C. Tully

Princeton University, Princeton, NJ, USA

A. Bodek, P. de Barbaro, H. Budd, Y. Chung, T. Haelen

University of Rochester, Rochester, NY, USA

S. Hagopian, V. Hagopian, K. Johnson

Florida State University, Tallahassee, FL, USA

V. Barnes, A. Laasanen

Purdue University, West Lafayette, IN, USA

Abstract

The response of the CMS combined electromagnetic and hadron calorimeter to beams of pions with momenta in the range 5 – 300 GeV/c has been measured in the H2 test beam at CERN in 2004. The raw response with the electromagnetic compartment calibrated to electrons and the hadron compartment calibrated to 300 GeV/c pions may be represented by $\sigma = (1.2)\sqrt{E} \oplus (0.095)E$. The fraction of energy visible in the calorimeter ranges from 0.72 at 5 GeV/c to 0.95 at 300 GeV/c, indicating a substantial nonlinearity. The intrinsic electron to hadron ratios are fit as a function of energy assuming a parametrized form for the neutral fraction of a hadronic shower and are found to be in the range 1.3 – 2.7 for the electromagnetic compartment and 1.4 – 1.8 for the hadronic compartment. The fits are used to correct the non-linearity of the e/π response to 5% over the entire measured range resulting in a substantially improved resolution at low energy. Longitudinal shower profiles have been measured in detail and compared to GEANT4 models, LHEP-3.7 and QGSP-2.8. At energies below 30 GeV, the data, LHEP and QGSP are in agreement. Above 30 GeV, LHEP gives a more accurate simulation of the longitudinal shower profile.

1 Introduction

The physics program for the Compact Muon Solenoid (CMS) [1] requires the detailed measurement of quark and gluon jets produced in pp collisions at the Large Hadron Collider (LHC) [2] at a center-of-mass energy of 14 TeV. The CMS spectrometer consists of a 4T superconducting solenoidal magnet of length 13 m and inner diameter 5.9 m. Located inside the coil are silicon pixels and strips for charged particle tracking [3], lead-tungstate crystals (ECAL) [4] to measure electromagnetic showers from electrons and photons, and a brass-scinitillator calorimeter to measure hadron showers (HCAL) [5, 6]. Muon chambers are embedded in the iron return yoke of the magnet outside the coil [7]. Jets will be reconstructed and triggered by their combined energy deposits ECAL plus HCAL over a wide energy range from several tens of GeV to several TeV [8]. The particle content of the jets arising from the fragmentation of quarks and gluons contains a significant number of low energy particles at scale of a few GeV. Since the electromagnetic calorimeter was designed for the best possible photon and electron energy resolution, compensation cannot be achieved, so that the response of CMS to electrons differs from that to pions in a substantial and energy dependent fashion. Low energy particles limit the energy resolution of jets due to the nonlinearity of the calorimeter response. The situation can be alleviated if knowledge of the identity of the localized energy deposits in the calorimeters can be achieved. Fortunately, the good calorimeter segmentation in azimuth (ϕ) and pseudorapidity (η) (0.017×0.017 and 0.087×0.087 in $\phi \times \eta$ for ECAL and HCAL, respectively), together with the excellent charged particle tracking will allow response corrections to be made within the jet to improve the resolution.

In order to achieve the CMS physics goals, it is important to understand the response of the calorimeter to low energy pions, and to have a reliable Monte Carlo program that can accurately simulate these results. Previously available test beam data have only spanned the momentum (p) interval $30 \leq p \leq 300$ GeV/c [6]. In 2004, a tertiary beam was commissioned in the CERN H2 beam line in the North Area. This beam covered the momentum range $2 \leq p \leq 9$ GeV/c. Momenta below 5 GeV/c, however, were judged to be too contaminated by backgrounds and not used in this analysis. Improved particle identification was then planned for the 2006 test beam run. In addition, beam-line instrumentation was installed and commissioned which allowed for clean beam particle identification of the secondary beam from $10 \leq p \leq 30$ GeV/c. This allowed for an approximate momentum overlap of tertiary and secondary beam data. The goal of the measurements described here is to measure the response of the calorimeter to single particles over the range $5 \leq p \leq 300$ GeV/c and to compare them to the GEANT4.

2 Experimental Setup

2.1 Calorimeter

The design of the HCAL barrel (HB) wedges is described in [6]. Each HB wedge is a sampling calorimeter with 17 layers of plastic scintillator, divided into 4 ϕ and 16 η sectors. The total absorber thickness at normal incidence ($\eta = 0$) is 5.38 absorption lengths ($\lambda_{\rm I}$). The effective thickness increases with $|\eta|$, such that at $|\eta| = 1.3$, the effective thickness is $11.6\lambda_{\rm I}$. Two HCAL barrel wedges (HB) were placed on a movable table. The movable table was designed to pivot about a position along the beam line to mimic the directions of particles originating from the CMS interaction point in the LHC. The moveable table was designed in such a way that it appears as if the beam is coming from the interaction region as it would at the CMS interaction point in the LHC. The table allows movement in both the ϕ and η directions. Most of the data for this study was taken at $\eta = 0.566$, where the thickness is $6.3\lambda_{\rm I}$.

The relative calibration of each HCAL scintillator was determined using a moving-wire radioactive source [9] and independently checked at the few percent level with muons. The uncertainty in the cell-to-cell relative calibration was 2.0% for the bottom wedge (HB1) and 2.6% for the top wedge (HB2). The resulting contribution to the linearity is less than 1.6%. The absolute energy scale was calibrated with a 50 GeV/c pion beam by summing the energies in a 3×3 array of ϕ, η segments, and requiring only a minimum-ionizing particle (*mip*) in ECAL. The mean energy deposited by a *mip* in ECAL is measured to be 400 MeV. The statistical error on the energy scale is $\pm 0.25\%$. The systematic error comes mainly from particles that interact in the dead material between ECAL and HCAL, and is estimated to be about 0.6%.

The photodetectors are hybrid photo diodes (HPD) [10] which have 19 separate light sensing channels or pixels. The readout electronics are comprised of charge integrator and encoder (QIE) [11], HCAL trigger and readout module (HTR) and data concentrator [12] (DCC). All of the digital electronics that were used in the test were production versions running at a clock speed of 40.079 MHz. One of the two HB wedges (HB1) was configured according to the CMS design, such that light from all scintillator tiles in each ϕ, η segment was summed optically and routed to one pixel of an HPD photodetector (Figure 1). Thus, this configuration has only transverse segmenta-

tion, and no longitudinal segmentation. The second HB wedge (HB2) was configured to measure the longitudinal shower development in the calorimeter. This was implemented by replacing the normal optical decoding units (ODUs) in the readout box with special ODUs. Due the limited number of HPD channels available in a readout box, this special ODUs summed the light from the scintillator tiles along η at the same depth in the center HCAL η segments (5-9). The remaining η segments were optically masked out to reduce the possible contribution from halo muons (Figure 1). The resulting energy measurements from each of 17 HCAL layers provided the complete HCAL longitudinal sampling of the hadron shower.

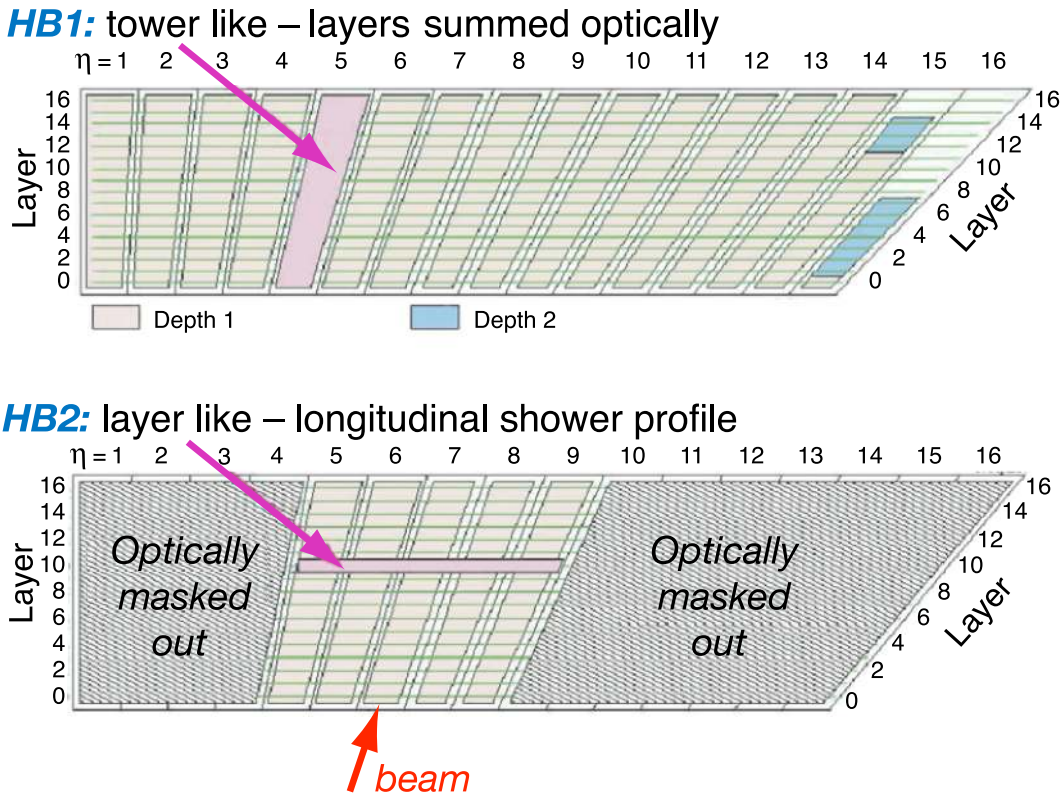

Figure 1: Readout segmentation for the two HB wedges. HB1 has the standard CMS readout configuration while HB2 has a special longitudinal readout of each scintillator layer.

An electromagnetic barrel prototype (EBP) module was placed in front of the HCAL on the moveable table. The EBP consisted of a 7×7 matrix of lead-tungstate crystals. Each crystal is a quadrilateral prism with a depth of 23 cm, a square front surface 20.5×20.5 mm^2, and a square rear surface 23.8×23.8 mm^2. The crystal thickness corresponds to 25.8 radiation lengths and $1.1\lambda_{\mathrm{I}}$. Each crystal was read out individually with a phototube through a light guide mounted on its front surface. An 8-cm aluminium block was placed between the EBP and HCAL modules to simulate the material in the ECAL electronics at that location in the CMS detector. Note that the EBP does not achieve the ultimate CMS ECAL performance. However, for jet studies the EBP energy resolution is sufficiently good.

2.2 H2 Beam Line

The 2004 HCAL Test Beam studies were conducted in the H2 test beam in the North Area at CERN. Two configurations of the beam line (Figure 2) were used. For particles with momenta in the range $10 \leq p \leq 300$ GeV/c, the normal configuration of H2 was used. The primary proton beam from the Super Proton Synchrotron (SPS) accelerator with $p = 400$ GeV/c strikes the primary target T2. Downstream from the primary target, a secondary hadron or electron beam is made in the momentum range $10 \leq p \leq 300$ GeV/c. To generate beams of particles with $p < 10$ GeV/c, an additional target (T22) and a beam stop were inserted into the beam line (Figure 2). Additional beam focusing and bending elements were introduced along the very low energy (VLE) path in order to make a well-defined beam with $2 \leq p \leq 9$ GeV/c from particles produced at T22.

A set of scintillation counters in the H2 beam line were used to provide trigger and particle identification informa-

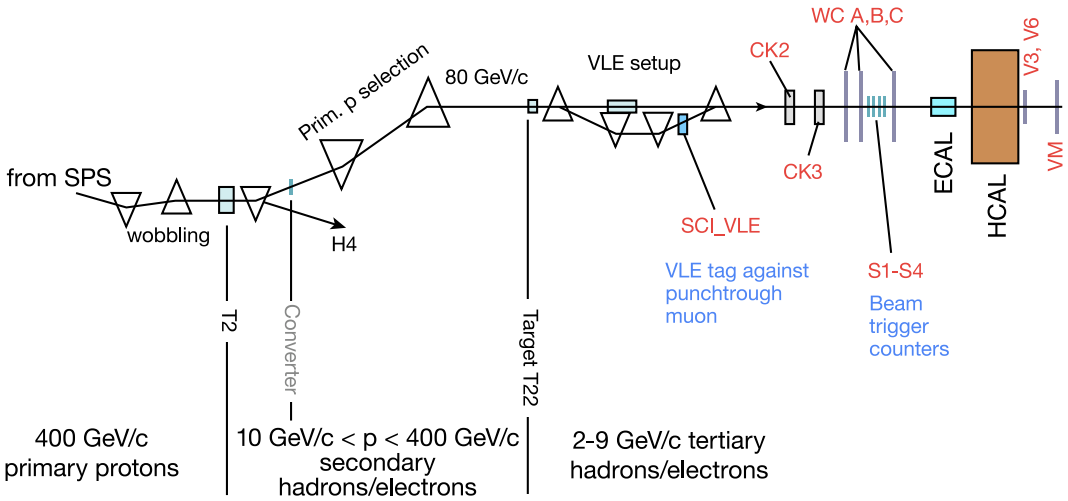

Figure 2: Primary elements defining the CERN H2 test beam in 2004.

tion. Trigger signals were created using four scintillators of different sizes: $14 \times 14 \times 1$ cm^3 (S1), $4 \times 4 \times 1$ cm^3 (S2), $2 \times 2 \times 1$ cm^3 (S3), and $14 \times 14 \times 1$ cm^3 (S4). Most of the data was taken with a 4×4 cm^2 beam size defined by the combination of S1, S2, and S4 in coincidence. Additional scintillators (V3, V6, and VM) were located behind the calorimeters to identify muons.

Particle identification was performed with Cherenkov counters CK2 and CK3. The gas pressure in CK2 was adjusted to positively identify electrons and so that pions with $p < 20$ GeV/c emit no Cherenkov light. CK3 was used to veto protons and kaons in the positively charged beams with $5 \leq p \leq 9$ GeV/c. The gas pressure in CK3 was set to give signals from pions with $p > 3.5$ GeV/c, muons with $p > 2.65$ GeV/c, kaons with $p > 12.4$ GeV/c, and protons with $p > 23.5$ GeV/c, so that only pions were positively tagged in the VLE beam.

Particles that interacted along the beam line before the calorimeters were indentified by multiple hits in a set of three wire chambers, each with active area 10×10 cm^2. All three wire chambers have two perpendicular planes of wires to measure the horizontal and verticle coordinate of any charged particle traversing the chamber. All three chambers had multi-hit electronics allowing the detection of showers from the upstream interaction of particles along the beam line. In the VLE configuration of the beam line, an additional scintillator (SCI_VLE, see Figure 2) was included to assure that the beam particle followed the VLE path during the very low energy data taking. This was necessary to eliminate muons created in the beam dump just after the T22 secondary target.

The data were used to estimate the counter efficiencies to be 99% for the muon counter VM, 92% for the CK2, 98% for the CK3, and 71% for each plane of the wire chambers.

2.3 Data Sets

Since the negatively charged beams have a negligible antiproton content, π^- beams were used to best measure the pion response of the calorimeter. To select pions, cuts are made on signals in the VLE muon counter (SCI_VLE), CK2 and CK3, and the muon scintillators (V3, V6, and VM). To partially remove the upstream beam line interactions, a cut is placed on the fraction of energy deposited in the HCAL ϕ, η segment which is aligned with the beam ($> 10\%$).

Three types of particle beams were used: pions, electrons, and muons. The available beam momenta, detector configurations, and data sets were as follows:

1. negative pion beams with 5, 7, and 9 GeV/c momenta in HB1 and HB2 with and without EBP in front of HCAL;
2. negative pion beams with 10, 15, 20, 30, 50, 100, 150, and 300 GeV/c momenta in HB1 and HB2 with and without EBP in front of HCAL;
3. electron beams with momentum 9 and 100 GeV/c which were directed into every HCAL and ECAL ϕ, η segment; and

4. muon beams with 150 GeV/c which were directed into every HCAL ϕ, η segment.

The 30 – 300 GeV/c data sets were taken early and did not yet include the muon veto counter (VM). Nevertheless, muons in this data set can be distinguished from hadron and electron showers in the calorimeter since they leave only minimum ionizing energy in the calorimeter, about 0.4 GeV in the EBP and 2.5 GeV in the HB. The high voltage on the phototubes and HPD photodetectors was set to nominal values for the EBP (–1200 V) and HCAL (8 kV). For the 5 – 15 GeV/c data, the gain of the photodetectors was increased (EBP –1500 V, HCAL 10 kV), in order to help suppress noise interfering with the smaller signals at these low beam momenta. Dedicated runs with the two different high voltages were used to measure the increase in the photodetector gains.

2.4 Simulation with GEANT4

The CMS software framework was used for the Monte Carlo simulation of the test beam [13]. The test beam is implemented as a standard CMS package with its own geometry description,and with the event information stored in ROOT ntuples [14]. The EBP plus HCAL geometry was implemented in GEANT4 [15]. An aluminium block of 8-cm thickness simulating the CMS cryostat and coil was located behind the wedges, followed by the HO scintillator layers. The EBP calorimeter was implemented as a single $PbWO_4$ crystal representing the 7×7 crystal matrix. In addition, all upstream material in the vicinity of the calorimeters was included in the GEANT4 geometrical description, including the trigger scintillators S1-S4 and wire chambers in order to study the interactions along the beam line.

The GEANT4 program supports a number of models of the processes that may be used to describe the details of the particle interactions. The test beam data reported here are compared to the LEP/HEP parameterized models for inelastic scattering (LHEP 3.7) and the quark gluon string model (QGSP 2.8) [15]. The data from HB2 were used to make detailed comparisons with the different GEANT4 models in regards to hadron shower depth distributions.

3 Response and Resolution

3.1 Pion Response

Figure 3 shows plots of measured energy in HCAL *vs.* measured energy in EBP for negatively charged pion beams of momenta 300, 100, 50, 30, 15, 10, 9, 7, and 5 GeV/c. After making the preliminary pion selection cuts (Section 2.3) using the Cherenkov and scintillation counters, the beam is still contaminated by muons and electrons as well as particles interacting upstream of the calorimeters. The contamination from muons and electrons becomes progressively worse at lower momentum. Residual electron contamination of the pion beam was reduced by applying a cut on the energy deposited in ECAL (vertical lines in Figure 3.1). Muons are suppressed by applying a cut on the weighted sum of the EBP and the HCAL signal. For the high momentum data (10 – 300 GeV/c), this cut is on a linear combination of the EBP and HCAL energy, while for low beam momenta (5 – 9 GeV/c), the cut is elliptical as shown in (Figure 3.1). The results are relatively insensitive to the value of the cuts, contributing only to the systematic uncertainty of the energy measurement. We note that in spite of the cuts described above, there is still a small contribution of events with very little energy deposited in ECAL together with low energy in HCAL indicating some contamination from upstream interactions. The outer calorimeter is also not used in this sample to correct for shower leakage.

The distributions of total energy in EBP plus HCAL (dN/dE) for various pion beam momenta are shown in Figure 4. Also shown for comparison are calculations of dN/dE using GEANT4 with LHEP and QGSP models. The overall agreement is good with some deviation of the Monte Carlo prediction from the measured response at the lowest energies (5 – 9 GeV/c). The mean and standard deviation of the measured response and GEANT4 predictions (LHEP and QGSP) are summarized in Table 1.

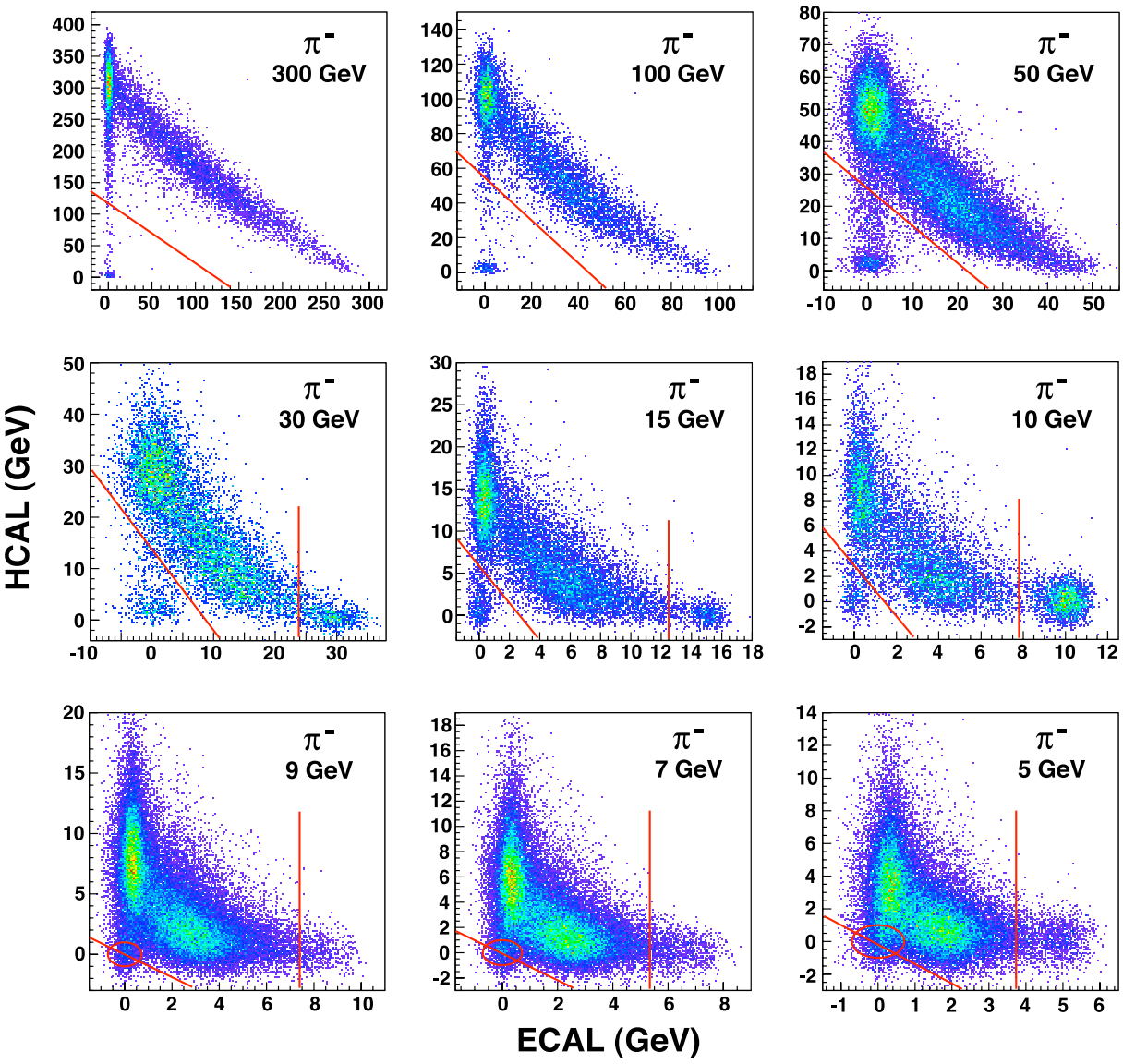

Figure 3: Energy observed in HCAL *vs.* energy observed in EBP for beams of 300, 100, 50, 30, 15, 10, 9, 7, and 5 GeV/*c* pions. Cuts used to reject electrons (vertical lines) and muons (diagonal lines and ellipses) are indicated. A long "tail" with little EBP energy and reduced HCAL energy due to upstream interactions is also evident.

Table 1: Sample mean and standard deviation of the EBP plus HCAL raw response and comparison to GEANT4 Monte Carlo calculations (LHEP and QGSP) for pions of 5, 7, 9, 10, 15, 30, 50, 100, and 300 GeV/c momenta. The data and Monte Carlo are not corrected for the intrinsic response ratio for electrons and hadrons.

	Data (GeV)		LHEP (GeV)		QGSP (GeV)	
p (GeV/c)	mean	σ	mean	σ	mean	σ
5	3.6	2.0	3.7	2.1	3.7	2.0
7	5.2	2.6	5.3	2.5	5.3	2.5
9	6.7	3.0	6.8	2.8	6.9	2.9
10	7.8	3.0	7.7	3.0	7.7	2.9
15	12.5	3.9	12.3	3.9	12.4	3.9
30	26.5	6.5	26.1	6.6	26.6	6.5
50	45.9	8.7	45.9	9.0	45.6	8.7
100	93.7	13.8	94.0	14.1	93.9	13.5
300	286	35	284	33	288	32

Figure 4 shows the average total observed energy in the calorimeter as a function beam momentum. This is the raw response with EBP calibrated to electrons and HCAL calibrated to 300 GeV pions. In the next section we discuss corrections to the linearity as abstracted from the data.

Figure 5 shows the reconstructed (uncorrected) fractional energy resolution *vs.* true pion beam energy (E). The resulting resolution is shown in Figure 6. The data may be fit to the form

$$\sigma = (1.2)\sqrt{E} \oplus (0.095)E \, , \tag{1}$$

where the symbol $\oplus$ denotes addition in quadrature of the stochastic and constant terms.

3.2 Response Corrections

The response of a non-compensating calorimeter to hadrons is known to be dependent on the fluctuations in the number of π^0s produced, which grows logarithmically with energy. The calorimeter may be described in terms of an intrinsic response ratio for electrons and hadrons in EBP $(e/h)_{\rm E}$ and HCAL $(e/h)_{\rm H}$. In this section, we describe the procedure by which the data were used to determine the values of $(e/h)_{\rm E}$ and $(e/h)_{\rm H}$. The observed energy-dependent response ratio for electrons and pions in EBP $(e/\pi)_{\rm E}$ and HCAL $(e/\pi)_{\rm H}$ may be written as a weakly energy-dependent function of $(e/h)_{\rm E}$ and $(e/h)_{\rm H}$ and the electromagnetic fraction of the hadron shower, f_0, due to the production of π^0s [16]:

$$(e/\pi)_i = \frac{(e/h)_i}{1 + [(e/h)_i - 1]f_0} \quad (i = \text{E or H}) \tag{2}$$

Knowledge of the functions $(e/\pi)_{\rm E}$ and $(e/\pi)_{\rm H}$ may then be used to correct the observed responses to pions in a combined EBP plus HCAL, which are refered to as $\varepsilon_{\rm E}$ and $\varepsilon_{\rm H}$, respectively. The absolute scale of $\varepsilon_{\rm E}$ is calibrated with electron beams, while the $\varepsilon_{\rm H}$ is calibrated with 300 GeV/c pions that are non-interacting in ECAL. The corrected pion energy (E) may be written as

$$E = (e/\pi)_{\rm E}\varepsilon_{\rm E} + \frac{(e/\pi)_{\rm H}}{(e/\pi)_{\rm H300}}\varepsilon_{\rm H} \, , \tag{3}$$

where $(e/\pi)_{\rm H300}$ is the value of $(e/\pi)_{\rm H}$ at 300 GeV where the HCAL energy scale is calibrated. The experimental error (σ) on our direct measurement of E in response to pions may be represented by

$$\sigma(E) = (0.80)\sqrt{E} \oplus (0.066)E \, . \tag{4}$$

We first describe a fitting procedure which allows $(e/h)_{\rm E}$ and $(e/h)_{\rm H}$ to depend on energy, and then later fix them to be constants for comparison of the resulting linearity after corrections are made. We express the intrinsic response ratio of HCAL as

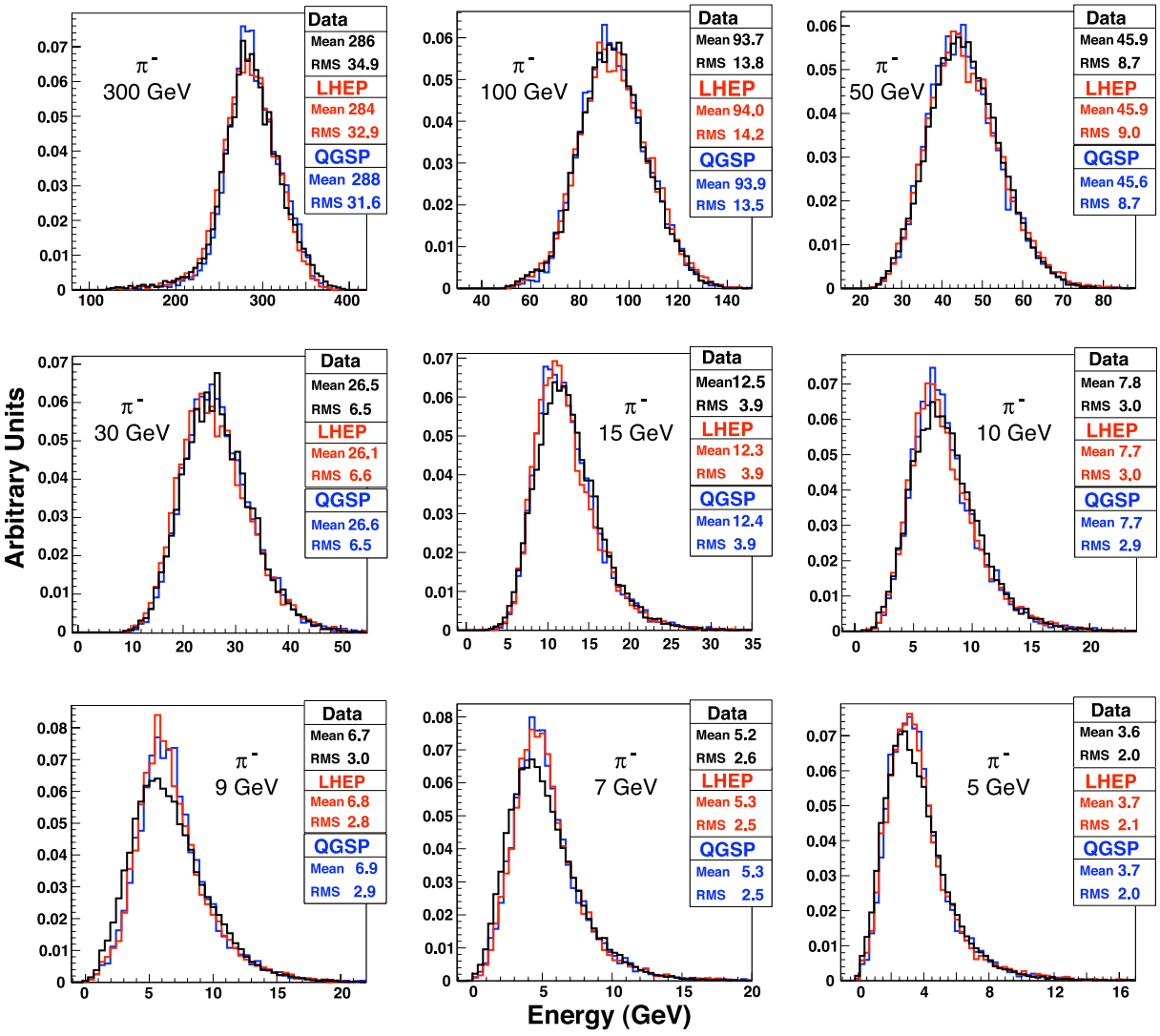

Figure 4: Total uncorrected energy observed in the calorimeter (EBP plus HCAL) with GEANT4 comparison for pions at various beam momenta.

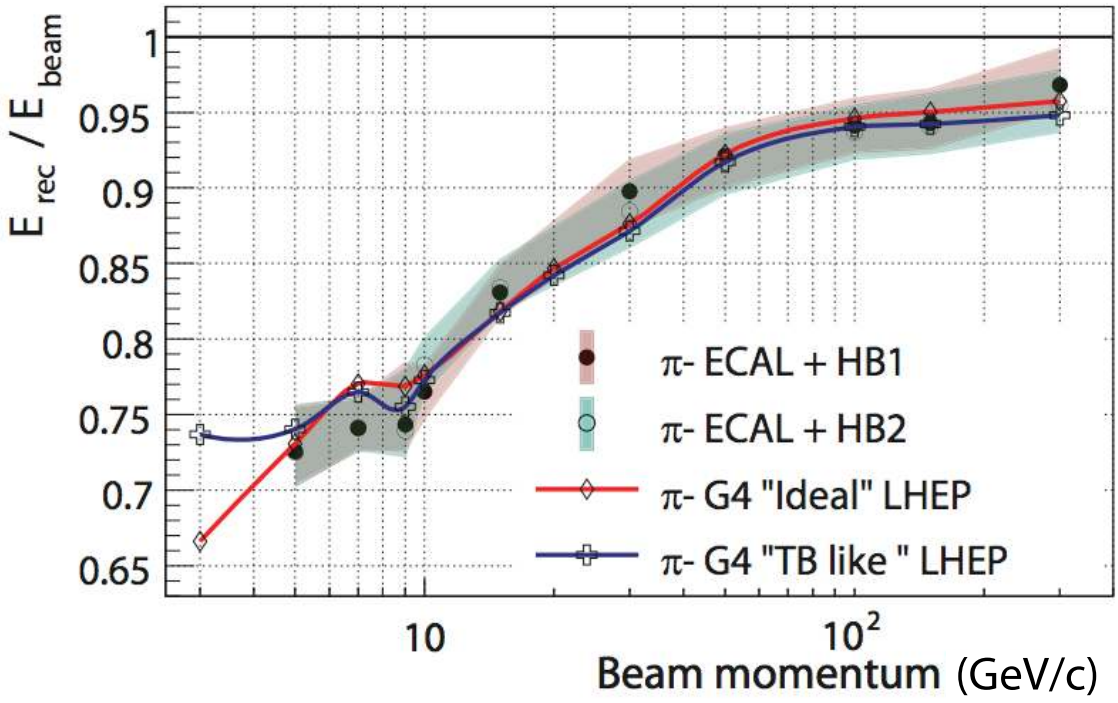

Figure 5: Reconstructed energy fraction recorded in EBP + HCAL *vs.* beam momentum.

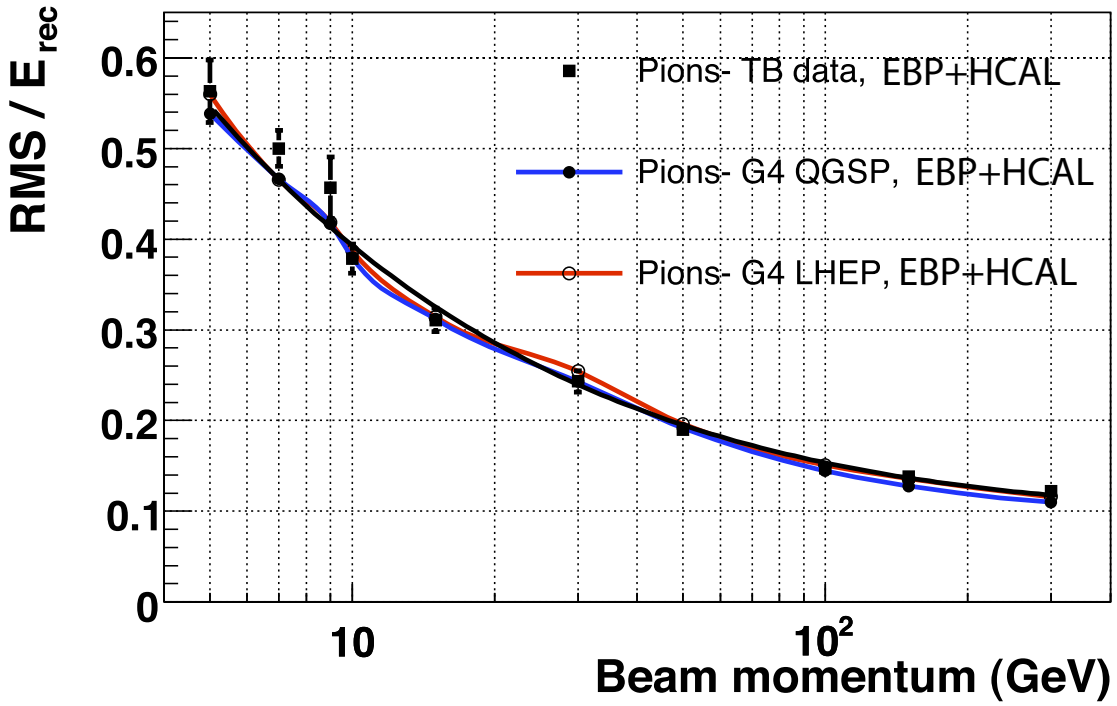

Figure 6: Reconstructed fractional energy resolution *vs.* beam momentum. The fit to the data points results in energy resolution which is described by $\frac{1.21}{\sqrt{E}} \oplus 0.095$ (black solid line).

$$(e/h)_{\rm H} = 1.39[1 + \frac{a_1}{\varepsilon_{\rm E} + \varepsilon_{\rm H}}] \,, \tag{5}$$

where the value of the constant term (1.39) is determined directly with beams of electrons sent into HCAL with EBP removed, and the constant a_1 may be nonzero due to a possible energy dependence of the response. The intrinsic response for ECAL, which cannot be directly measured due to its limited thickness (1.1λ), is similarly written as

$$(e/h)_{\rm E} = a_2[1 + \frac{a_3}{\varepsilon_{\rm E} + \varepsilon_{\rm H}}] \,. \tag{6}$$

We write the π^0 fraction as

$$f_0 = a_4[\ln(\varepsilon_{\rm E} + \varepsilon_{\rm H})]^{a_5}, \tag{7}$$

where the constant a_5 allows for the possibility of this fraction to deviate from a pure logrithmic behavior [17, 18].

Equations 5, 6, and 7 contain five unknown constants, $a_i (i = 1, ..., 5)$ that can be fit using pion data by minimizing the chi-squared (χ^2),

$$\chi^2 = \sum_i (\frac{p_0 - E_i}{\sigma_i})^2 \,, \tag{8}$$

where p_0 is the beam momentum, E_i is the corrected measured energy of an individual shower determined using Eq. 3, and σ_i is its error determined from Eq. 4. The fits were performed using EBP and HCAL raw energies from 500 pion showers for each of 4 beam momenta of 10, 30, 100 and 300 GeV/c. If no fit is made, $\chi^2 = 6860$ for 2000 degrees of freedom, while the 5 parameter fit gives $\chi^2 = 5760$ for 1995 degrees of freedom. There appears to be no significant systematic non-zero trend as a function of beam momentum. Clearly, there are events with large deviations which reflect the non-Gaussian tails in the resulting fit energy distributions. The Gaussian errors, however, do not appear to be seriously underestimated.

The best-fit values of $a_4 = 0.113$ and $a_5 = 0.872$ are close to those quoted in fits to the neutral fraction [18]. The resulting plot of f_0 as a funtion of energy is shown in Figure 7. The fit is compared to two well-known

parametrizations of f_0 [17, 18]. The values for the other parameters are $a_1 = 1.39$, $a_2 = 5.64$ and $a_3 = 1.26$. The ratios were found to be $(e/h)_{\rm E} = 1.28$ and $(e/h)_{\rm H} = 1.40$ at 300 GeV/c which increase to $(e/h)_{\rm E} = 1.97$ and $(e/h)_{\rm H} = 1.58$ at 10 GeV/c. The resulting energy-dependent pion response corrections, $(e/\pi)_{\rm E}$ and $(e/\pi)_{\rm H}$ are shown in Figure 8. The data show that the corrections are extremely important at low energy.

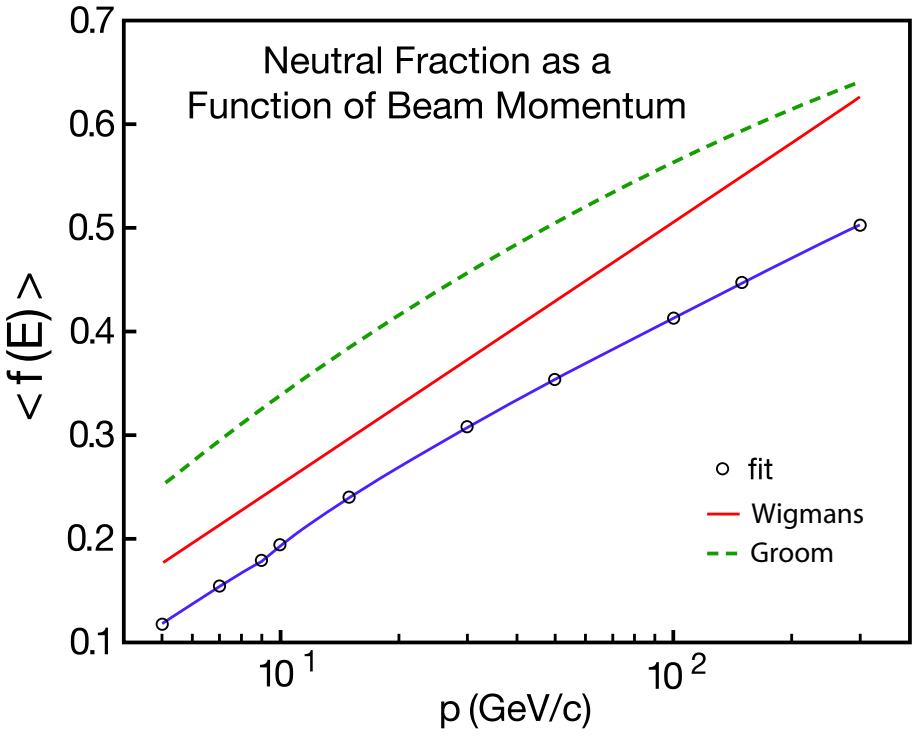

Figure 7: The average fraction of electromagnetic shower energy *vs.* beam momentum for data (open circles) and various fits (lines) [18].

The distribution of the raw energy sum, $\varepsilon_{\rm E} + \varepsilon_{\rm H}$, and the corrected energy sum, E, for a beam momentum of 15 GeV/c is shown in Figure 9. The mean measured raw energy is $\langle \varepsilon_{\rm E} + \varepsilon_{\rm H} \rangle = 11.3$ GeV with a root mean square (*rms*) deviation of 3.3 GeV or 29.4%. The poor linearity of the raw data is evident as a tail of the distribution at large energies. The size of the corrections to $\varepsilon_{\rm E}$ and $\varepsilon_{\rm H}$ is $(e/\pi)_{\rm E} = 1.46 - 1.75$ and $(e/\pi)_{\rm H} = 1.20 - 1.26$ for $\pm 1\sigma$ deviations from the mean raw response. The corrected energy distribution has a mean of $\langle E \rangle = 15.4$ GeV, indicating that the fitting procedure restores linearity as it was designed to do. The *rms* of 3.90 GeV, or 25%, in the corrected sample also shows that the fit improves resolution by pulling in the long tails toward the mean.

A scatter plot of the raw and corrected energies in EBP and HCAL is shown in Figure 10. A cut of 12.5 GeV which was imposed on the raw EBP energy to remove residual electron beam contamination is evident. It is easy to see in this plot what the corrections are doing. The HCAL energy is slightly increased to correct for non-compensation in the HCAL for those events where most of the energy is deposited in the HCAL. On the other hand, when most of the pion energy is deposited in ECAL a larger correction is needed as given by Eq. 2.

Fluctuations about the mean (Figure 9) are not dramatically improved with the energy corrections because the calorimetry is still non-compensating. Therefore, fluctuations in the neutral fraction (δf_0) will continue to cause fluctuations in the detected energy even though we can calibrate out the mean by correcting event by event. Treating the complete calorimeter as a simple homogeneous device, the fluctuations δf_0 due to all the hadronic interactions in the pion shower can be related to the resulting contribution to the energy measurement error ($\Delta E_f/E$) by

$$\frac{\Delta E_f}{E} \approx (e/h - 1)\delta f_0 \; . \tag{9}$$

The resulting fractional contribution to the energy error, $\Delta E_f/E$, is only weakly energy dependent. This error folds in quadrature with other contributions to the constant term 0.066 in Eq. 4, such as detector inhomogenity and photostatistics, and therefore does not dominate the overall constant term.

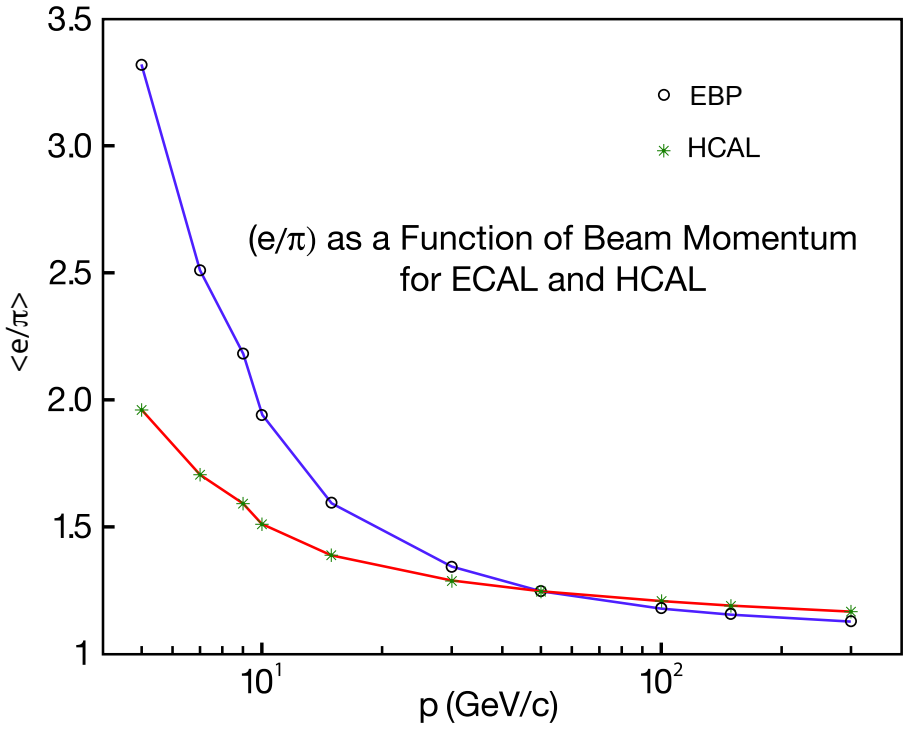

Figure 8: Response correction factors for EBP and HCAL, $(e/\pi)_{\rm E}$ and $(e/\pi)_{\rm H}$, as a function of beam momenta.

The fractional energy resolution for the raw data, the corrected data and the results of a Gaussian fit to the corrected data are shown in Figure 11. The correction improves the *rms* resolution, due to the equalization of the mean responses of the EBP and HCAL compartments of the calorimetry which then removes fluctuations due to event by event changes in the EBP/HCAL energy partition. This same effect was seen in Figure 10. In addition, the response is made more Gaussian (see Figure 9), which is reflected in an improvement of the sample *rms* with respect to the σ with a Gaussian fit.

The resulting linearity is shown in Figure 12. To further investigate the calorimeter response, we performed a one parameter fit to a_2 by fixing the values $a_1 = 0$, $a_3 = 0$, $a_4 = 0.11$, and $a_5 = 1$. This has the effect of fixing the intrinsic response ratios, $(e/h)_{\rm E}$ and $(e/h)_{\rm H}$, as constants, and putting all the energy dependence of the response into f_0. The result of this fit gives $a_2 = 2.0$. The 5 parameter fit gives a smaller value of χ^2 because the errors are large for low momenta. The one parameter fit, however, gives linearity closer to one over a wider momentum range. Which algorithm is adopted may depend on the particular analysis which is under study. For example, the *rms* errors of Eq. 4 can be tuned to emphasize an energy range of interest to a particular analysis. In any case, the linearity of the EBP plus HCAL is restored at the 5% level for momenta above about 10 GeV/c.

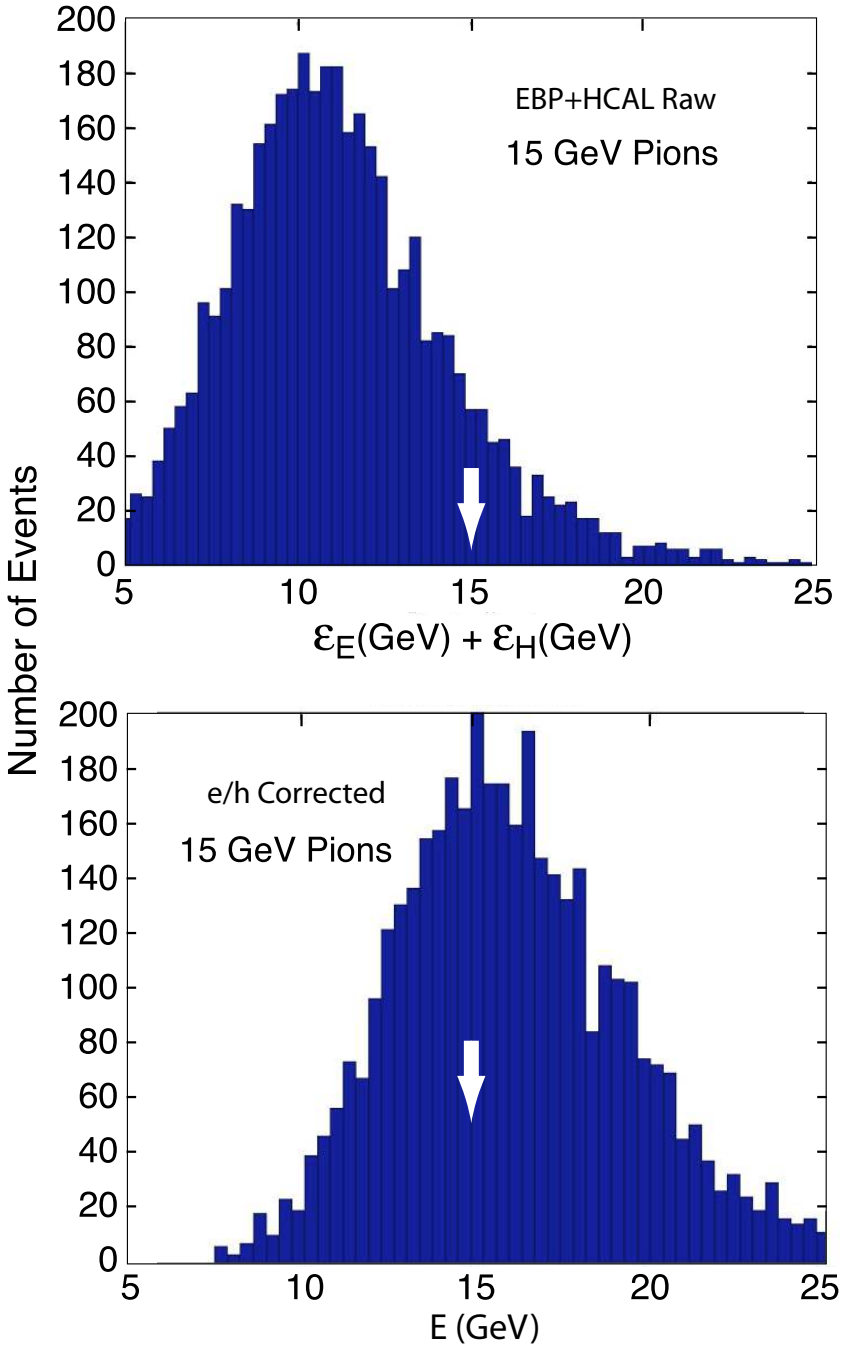

Figure 9: : Distribution of (top) raw total energy and (bottom) corrected total energy for 15 GeV/c incident pions. The arrow indicates the beam momentum.

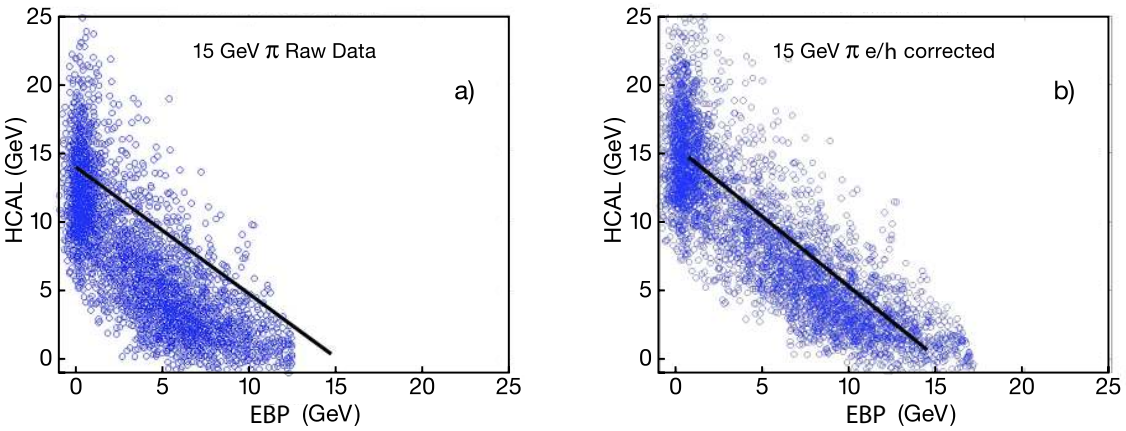

Figure 10: Plot of HCAL energy *vs.* EBP energy for the 15 GeV/*c* incident pion beam data. The plots are shown for (a) raw data and (b) corrected data. Electron contamination in the data has been removed by imposing a cut on the maximum allowed raw ECAL energy. The lines indicate the average behavior of a linear calorimeter.

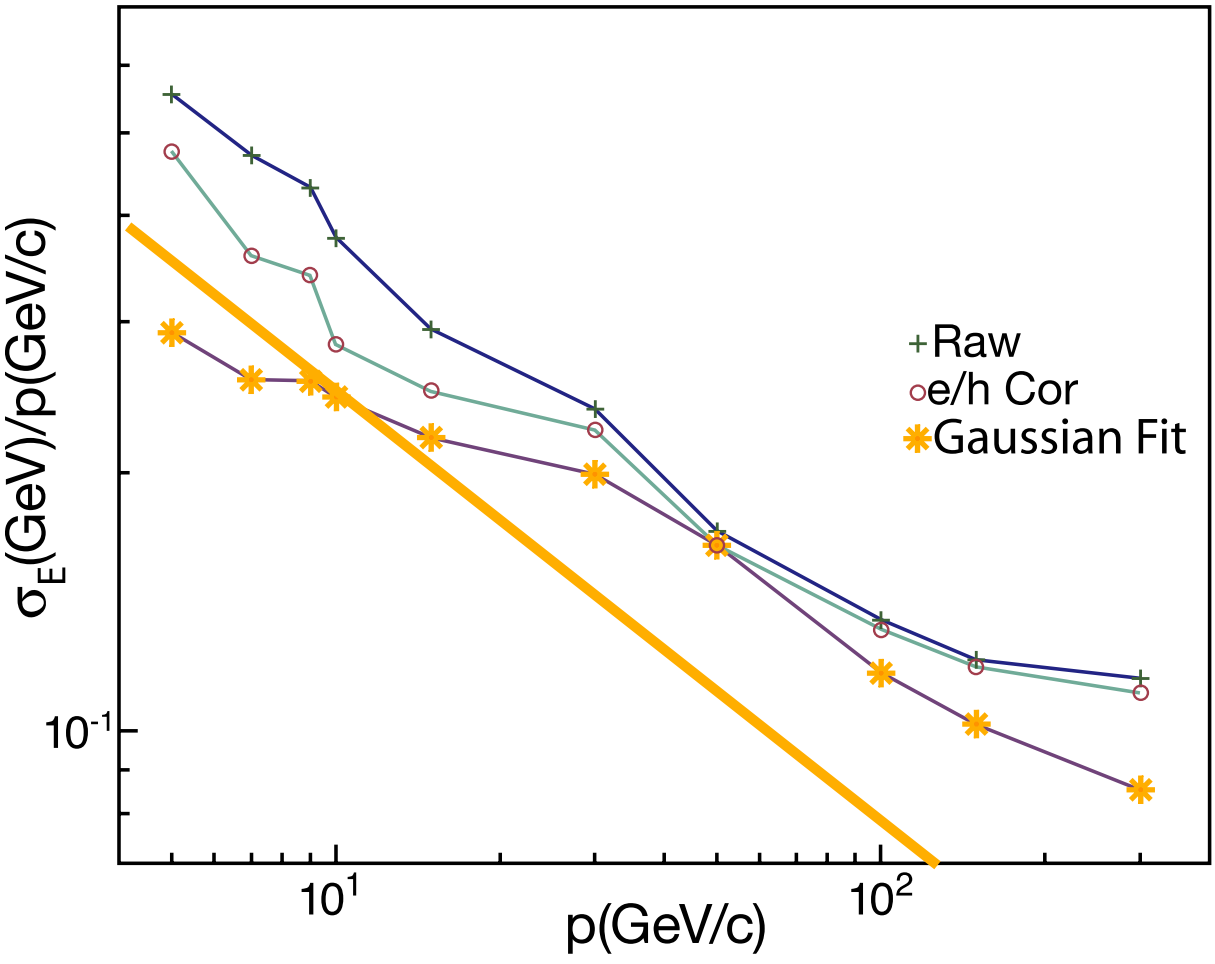

Figure 11: Fractional energy resolution for raw, corrected and Gaussian fitted corrected data as a function of beam momentum from 5 to 300 GeV/*c*. The thick line indicates a stochastic resolution of 80% (Eq. 4).

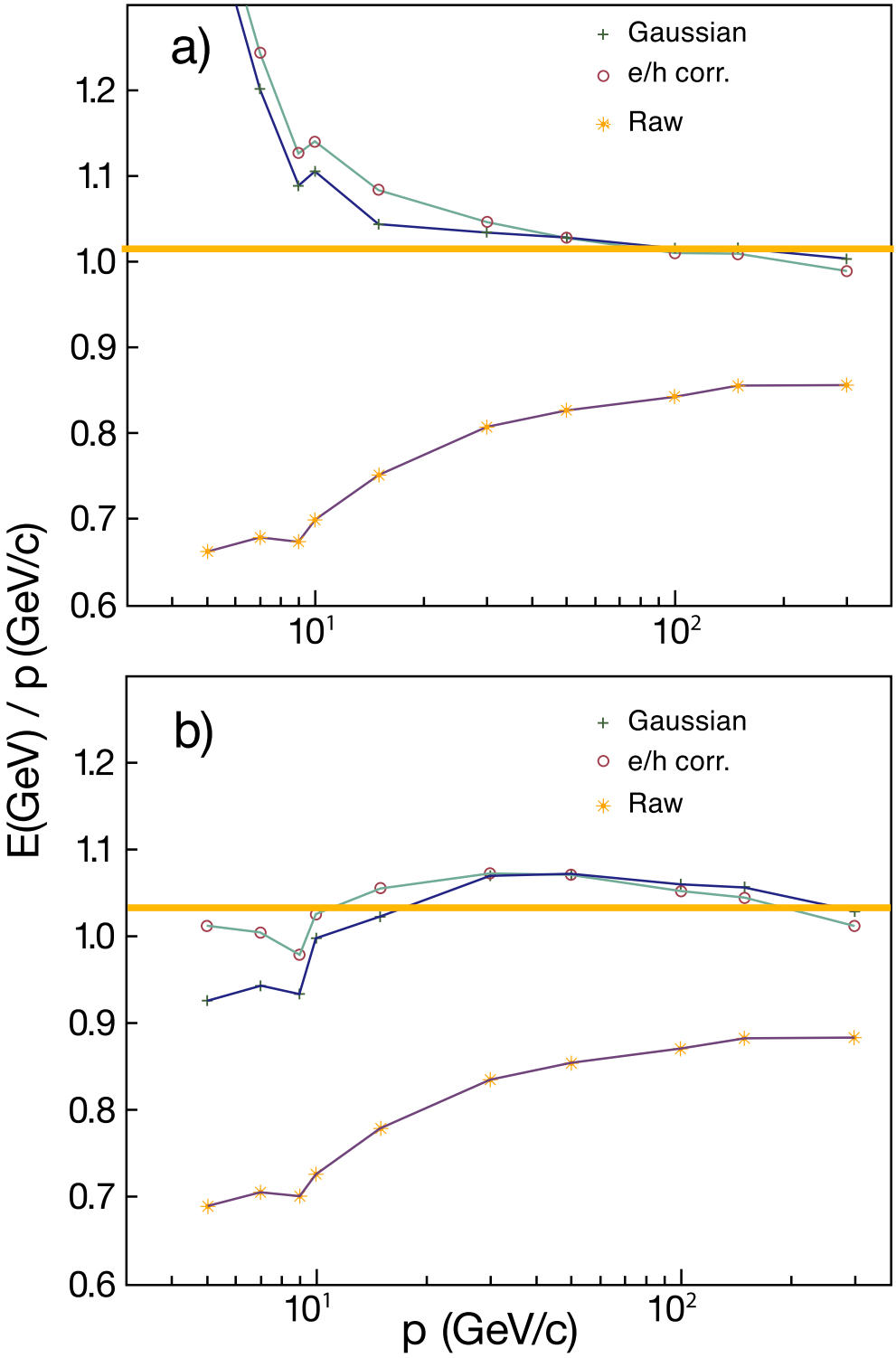

Figure 12: Mean energy response for raw data, corrected data and Gaussian fitted corrected data as a function of beam momentum. The line indicates a linear device, EBP plus HCAL. a) five parameter fit and b) one parameter fit.

4 Longitudinal Profile

The sum of energies in a matrix of 3×5 (ϕ, η) segments at each depth was used to measure the deposited energy from pions to investigate the longitudinal shower development. This ensures full shower containment in the transverse plane. For this measurement, we select pions that do not interact in EBP or the aluminum block in front of HCAL by requiring minimum ionization in EBP ($\varepsilon_E < 0.4$ GeV) and a small energy deposition (< 0.7 GeV) in Layer-0 of HCAL.

Figure 13 shows the measured longitudinal profile for different beam momenta and also displays comparison with GEANT4 LHEP and QGSP models. The location of the shower maximum increases from layer 1 at 5 GeV/c, to layer 5 at 300 GeV/c. Overall, GEANT4 simulates the test beam data well. The QGSP physics list shows a shorter shower profile at 100 – 300 GeV/c beam momentum, which explains why the reconstructed energy is larger due to smaller leakage out the back of the HCAL. At momenta below 50 GeV/c, both LHEP and QGSP show good agreement with the test beam data and with each other.

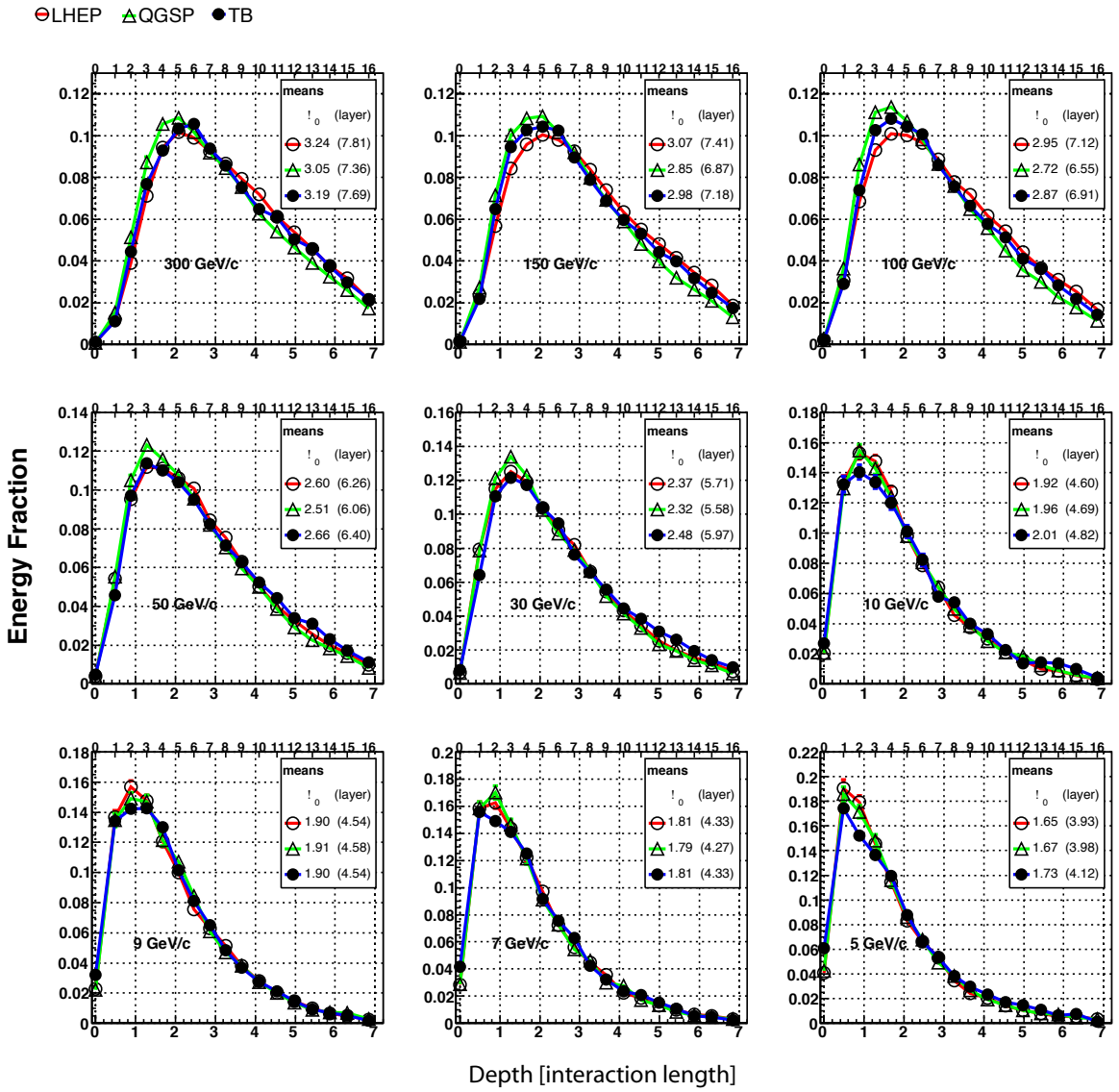

Figure 13: Longitudinal energy profile observed in HCAL in comparison to GEANT4 for beams of 300, 150, 100, 50, 30, 10, 9, 7, and 5 GeV/c pions.

The HPD has a cross-talk between pixels in the absence of a magnetic field. The magnitude of such cross-talk is defined as the fraction of the charge of a pixel which is collected by each of its neighbor pixels. This fraction is

estimated to be in the 1 – 2% range for the most of the pixel pairs. The cross-talk is estimated from the electron data without EBP, where the back of the HCAL is expected to have no signal from electromagnetic showers. The HPD pixel layout for HB2 is shown in Figure 14, where it is seen that Layer-0 may receive cross-talk from layers 12, 13, and 16. If the energy in Layer-0 is not corrected for this cross-talk, it could bias the event selection, causing a shorter average shower profile by suppressing the events with showers which produce more energy in layers 12, 13, and 16. In order to reduce this bias, a correction is made to layer 0 (1.8%) to reduce its value to the most probable value measured with muons (0.15 GeV) where we assume that muons, on average, deposit minimum ionization in all layers in depth.

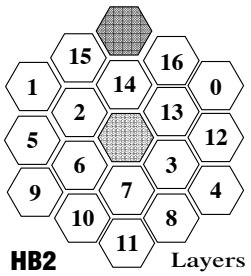

Figure 14: Pixel mapping for the longitudinal readout of HB2.

5 Summary

The CMS calorimeter components, a prototype electromagnetic compartment of lead-tungstate crystals designed and calibrated for good electron-photon resolution together with a brass-scintillator hadron sampling calorimeter calibrated with high energy pions, have rather large e/h intrinsic response ratios. This degrades the raw response of pions. especially at low energy, important for the measurement of jets. In order to measure and study the effect of e/h, modifications were made to the H2 beam line at CERN, allowing useable beams as low as 5 GeV/c. We have made detailed measurements of the EBP plus HCAL response to pions of momentum from 5 to 300 GeV/c.

The uncorrected response follows the form $\sigma = (1.2)\sqrt{E} \oplus (0.095)E$. The data have been used to fit the e/π response as a function of energy and thus determine the values of the intrinsic e/h to range from 1.3 – 2.7 for the ECAL crystals and 1.4 – 1.8 for the HCAL brass-scintillator over the energy range 300 – 5 GeV. These values are used to correct the linearity to approximately 5% uniformity over the entire measured energy range resulting in a substantially improved resolution at low energy ($\sigma = 25\%$ at 10 GeV).

Each of the 17 layers of HCAL was read out individually to provide a detailed measurement of the longitudinal shower profile as a function of shower energy. The GEANT4 Monte Carlo has been used to provide detailed simulations of the shower profile. The models LHEP-3.7 and QGSP-2.8 agree well with each other and provide a good representation of the shower profile at energies below 30 GeV/c. Above 30 GeV/c, LHEP gives a better simulation of the measured shower profile while QGSP gives a profile which is somewhat more compact.

References

[1] G. Baiatian *et al.*, "CMS Physics Technical Design Report, Vol. I: Detector Performance and Software," CERN/LHCC 2006-001, ed. D. Acosta (2006).

[2] The LHC design report and current status is available at http://lhc-new-homepage.web.cern.ch/lhc-new-homepage/.

[3] Tracker Technical Design Report, CERN/LHCC 98-6 (1998); "Addendum to the CMS Tracker TDR," CERN/LHCC 2000-016, CMS TDR 5 (2000).

[4] The Electromagnetic Calorimeter Technical Design Report, CERN/LHCC 97-33, CMS TDR 4 (1997).

[5] The Hadron Calorimeter Technical Design Report, CERN/LHCC 97-32 CMS TDR 3 (1997).

[6] G. Baiatian *et al*, CMS NOTE-2006/138.

[7] Muon Technical Design Report, CERN/LHCC 98-6 (1998).

[8] W. Adam *et al*, The CMS High Level Trigger, hep-ex/0512077 and Eur. Phys. J. C 46 605 (2006).

[9] E. Hazen *et al*, Nucl. Instr. and Meth. **A511** (2003) 311.

[10] P. Cushman, A. Heering, and A. Ronzhin, Nucl. Instr. and Meth. **A442** (2000) 289.

[11] T. Zimmerman and J. R. Hoff, IEEE J. Solid State Circuits, 39 (2004) 895.

[12] E. Hazen, J. Rohlf, S. Wu, A. Baden, and T. Grassi, Proceedings of the 7th Workshop on Electronics for LHC Experiments, Stockholm, CERN 2001-005 and CERN/LHCC/2001-034, 347 (2001).

[13] Object oriented Simulation for CMS Analysis and Reconstruction. http://cmsdoc.cern.ch/OSCAR/

[14] Proceedings of the AIHENP 1996 Workshop, Lausanne, Sep. 1996, Nucl. Inst. & Meth. A 389 (1997) 81. See also http://root.cern.ch/, Rene Brun and Fons Rademakers, ROOT - An Object Oriented Data Analysis Framework.

[15] S. Agostinelli *et al*, Nucl. Instr. and Meth. **A506** (2003) 250.

[16] R. Wigmans, Nucl. Instr. and Meth. **A265** (1988) 273.

[17] V. V. Abramov *et al*, Nucl. Instr. and Meth. **A457** (2001) 75.

[18] W.-M. Yao *et al*, Particle Data Group, "The Review of Particle Physics," Journal of Physics G 33, 1 (2006) available at http://pdg.lbl.gov/.